Geochemistry Geophysics Geosystems G3

Article
Volume 13, Number 8
9 August 2012
Q08002, doi:10.1029/2012GC004120
ISSN: 1525-2027

Published by AGU and the Geochemical Society

Pyrite alteration and neoformed magnetic minerals in the fault zone of the Chi-Chi earthquake (M_w 7.6, 1999): Evidence for frictional heating and co-seismic fluids

Yu-Min Chou
Department of Geosciences, National Taiwan University, 1 Roosevelt Road, Section 4, Taipei 106, Taiwan

Département Géosciences et Environnement, Université de Cergy-Pontoise, 5 mail Gay Lussac, Neuville sur Oise, FR-95031 Cergy-Pontoise CEDEX, France

Sheng-Rong Song
Department of Geosciences, National Taiwan University, 1 Roosevelt Road, Section 4, Taipei 106, Taiwan (srsong@ntu.edu.tw)

Associated International Laboratory, Active Deformation and Environment Programme for Taiwan, National Science Council, 106, Sec. 2, Heping East Road, Taipei 106, Taiwan

Charles Aubourg
Laboratoire des Fluides Complexes et Leurs Réservoirs, UMR5150, CNRS, TOTAL, Université de Pau, FR-64013 Pau CEDEX, France (charles.aubourg@univ-pau.fr)

Associated International Laboratory, Active Deformation and Environment Programme for Taiwan, National Science Council, 106, Sec. 2, Heping East Road, Taipei 106, Taiwan

Yen-Fang Song
National Synchrotron Radiation Research Center, 101 Hsin-Ann Road, Hsinchu Science Park, Hsinchu 30076, Taiwan (song@nsrrc.org.tw)

Anne-Marie Boullier
Associated International Laboratory, Active Deformation and Environment Programme for Taiwan, National Science Council, 106, Sec. 2, Heping East Road, Taipei 106, Taiwan

ISTerre, CNRS, Université Joseph Fourier, Maison des Géosciences, BP 53, FR-38041 Grenoble CEDEX 9, France

Teh-Quei Lee
Institute of Earth Sciences, Academia Sinica, 128, Section 2, Academia Road, Nankang, Taipei 115, Taiwan

Associated International Laboratory, Active Deformation and Environment Programme for Taiwan, National Science Council, 106, Sec. 2, Heping East Road, Taipei 106, Taiwan

Mark Evans
Department of Physics and Earth Science, Central Connecticut State University, New Britain, Connecticut 06050, USA

En-Chao Yeh

Associated International Laboratory, Active Deformation and Environment Programme for Taiwan, National Science Council, 106, Sec. 2, Heping East Road, Taipei 106, Taiwan

Department of Earth Sciences, National Taiwan Normal University, Number 88, Section 4, Tingzhou Road, Wenshan District, Taipei 11677, Taiwan

Yi-Ming Chen

National Synchrotron Radiation Research Center, 101 Hsin-Ann Road, Hsinchu Science Park, Hsinchu 30076, Taiwan

[1] During an earthquake, physical and chemical transformations lead to alteration and formation of minerals in the gouge layer. Altered and neoformed minerals can be used as tracers of some earthquake processes. In this study, we investigate pyrite and magnetic minerals within the host Chinshui siltstone and the 16-cm-thick gouge. This gouge hosts the principal slip zone of Chi-Chi earthquake (M_w 7.6, 1999). In the Chinshui siltstone, pyrite framboids of various sizes and euhedral pyrite are observed. The magnetic mineral assemblage comprises stoichiometric magnetite, greigite, and fine-grained pyrrhotite. The pyrite content is generally reduced in the gouge compared to the wall rock. The magnetic mineral assemblage in the gouge consists of goethite, pyrrhotite, and partially oxidized magnetite. The pyrrhotite, goethite and some magnetite are neoformed. Pyrrhotite likely formed from high temperature decomposition of pyrite (>500°C) generated during co-seismic slip of repeated earthquakes. Goethite is inferred to have formed from hot aqueous co-seismic fluid (>350°C) in association with the 1999 Chi-Chi event. Elevated fluid temperatures can also explain the partial alteration of magnetite and the retrograde alteration of some pyrrhotite to pyrite. We suggest that characterization of neoformed magnetic minerals can provide important information for studying earthquake slip zones in sediment-derived fault gouge.

Components: 9800 words, 8 figures, 1 table.

Keywords: Chi-Chi earthquake; TCDP; gouge; pyrite.

Index Terms: 3617 Mineralogy and Petrology: Alteration and weathering processes (1039); 8010 Structural Geology: Fractures and faults; 8163 Tectonophysics: Rheology and friction of fault zones (8034).

Received 23 February 2012; **Revised** 12 June 2012; **Accepted** 12 June 2012; **Published** 9 August 2012.

Chou, Y.-M., S.-R. Song, C. Aubourg, Y.-F. Song, A.-M. Boullier, T.-Q. Lee, M. Evans, E.-C. Yeh, and Y.-M. Chen (2012), Pyrite alteration and neoformed magnetic minerals in the fault zone of the Chi-Chi earthquake (M_w 7.6, 1999): Evidence for frictional heating and co-seismic fluids, *Geochem. Geophys. Geosyst.*, *13*, Q08002, doi:10.1029/2012GC004120.

1. Introduction

[2] High-friction fault slip zones formed during earthquakes or laboratory experiments have distinguishable textures and mineral characteristics [*Nakamura et al.*, 2002; *Fukuchi et al.*, 2005; *Tanikawa et al.*, 2007; *Boullier et al.*, 2009]. In principle, characterization of slip zones may be relevant for assessing physical processes such as frictional heating, thermal pressurization, fracture energy, redox conditions, etc. In siliciclastic sedimentary environments, faults can develop within siltstones. These detrital rocks typically contain accessory minerals like siderite, iron oxides, and iron sulfides. Among these accessory minerals, pyrite (FeS_2) is worthy of study across slip zones for several reasons: 1) it is common within fine-grained sediments with a concentration of about 1% [*Berner*, 1984]; 2) it is easy to identify using optical microscopy or electron microscopy; 3) it generally has a euhedral morphology with well-calibrated size distributions [*Craig et al.*, 1998]; 4) pyrite crystals often cluster in so-called framboids that are as large as tens of microns across [*Craig et al.*, 1998]; 5) it alters rapidly with temperature and in the presence of certain fluids; and releases SO_4^{2-} and Fe^{2+} [*Jovanović*, 1989; *Music et al.*, 1992; *Lambert et al.*, 1998; *Pelovski and Petkova*, 1999; *Mayoral et al.*, 2002]; 6) pyrite alteration lowers pH, which can result in dissolution of carbonate minerals that can then reprecipitate in the gouge [*Liu and Liu*, 2004].

[3] In fault zones, magnetic minerals are of interest because magnetic susceptibility anomalies have been reported in gouge and pseudotachylites [*Nakamura et al.*, 2002; *Mishima et al.*, 2009; *Tanikawa et al.*, 2007; *Ferré et al.*, 2012]. Similarly, *Nakamura et al.* [2002] and *Ferré et al.* [2005] suggested that magnetic minerals form during frictional melting associated with fault displacement during earthquakes. Generally, magnetic minerals are difficult to observe using optical or electron microscopy because of their low concentration (<0.1%) and small grain size (<1 μm). However, it is relatively easy to determine the nature, size and concentration of magnetic minerals using rock magnetic methods [e.g., *Hunt et al.*, 1995]. Comparison between the magnetic mineral assemblage of wall rocks and fault gouge can help to determine the nature of neoformed magnetic minerals.

[4] During the Chi-Chi earthquake (M_w 7.6, 1999), a large ~80 km rupture occurred along the Chelungpu thrust [*Ma et al.*, 1999]. The Chelungpu thrust propagates through the siliciclastic early Pliocene Chinshui Formation where pyrite framboids are initially present in the undeformed sediment [*Boullier et al.*, 2009]. However, *Hirono et al.* [2008] reported a lack of pyrite in the gouge zone. Similarly, *Hirono et al.* [2007b] and *Ishikawa et al.* [2008] observed an abundance of SO_4^{2-} in the gouge zone and related it to pyrite dissolution. The gouge zone is also marked by a magnetic susceptibility peak due to the contribution of neoformed ferrimagnetic minerals [*Mishima et al.*, 2009]. There is, therefore, an apparent correlation between the lack of pyrite and neoformed magnetic minerals that we would like to elucidate. Using unaltered samples from the Taiwan Chelungpu-fault Drilling Project (TCDP) Hole B borehole [*Hirono et al.*, 2007a; *Song et al.*, 2007a; *Yeh et al.*, 2007], we determined how pyrite alter with the gouge and established the magnetic mineralogy of the Chinshui Formation and the gouge that hosts the 1999 Chi-Chi principal slip zone. The peak temperature reached in the gouge during the Chi-Chi earthquake is still debated; however, we show that identification of neoformed magnetic minerals provides additional evidence to estimate peak temperature and the presence of co-seismic fluids.

2. Geologic Setting

[5] In Taiwan, one of the largest inland earthquakes (M_w = 7.6) took place on 21 September 1999, near the town of Chi-Chi (hypocenter 120.81°E, 23.86°N, depth ~10 km [*Ma et al.*, 1999; *Kao and Chen*, 2000], which caused large-scale casualties (2,321 deaths, 10,000 injured) and destruction (more than 100,000 buildings were damaged or destroyed). During the 1999 Chi-Chi earthquake, the surface rupture closely followed the ~80 km Chelungpu fault, which is one of the most active faults in western Taiwan [*Chen et al.*, 2002]. The Chelungpu fault system is an out-of-sequence thrust (Figure 1a), which is part of the ramp of a ~20 km fault-bend-fold that is now largely eroded [*Yue et al.*, 2005; *Yeh et al.*, 2007]. The TCDP was designed to drill two cores in DaKeng, central Taiwan (Figures 1a and 1b) [*Yeh et al.*, 2007]. Hole A (depth 2,003 m) and Hole B (depth 1,352.6 m) are separated by 40 m. At the location of the two boreholes, the estimated slip during the 1999 Chi-Chi earthquake is ~8 m [*Ma et al.*, 2003]. Three major fault zones were identified within the Chinshui Formation [*Hirono et al.*, 2007a]. From independent data sets, different authors proposed that the fault zone at 1,111 m depth and 1,136 m depth for Hole A and B, respectively, contains the principal slip zone (PSZ) of the Chi-Chi earthquake [*Kano et al.*, 2006; *Ma et al.*, 2006; *Song et al.*, 2007a; *Wu et al.*, 2007; *Chou et al.*, 2012]. *Boullier et al.* [2009] determined the location of the Chi-Chi PSZ by identifying a ~2 cm (Hole A) to 3 mm (Hole B) thick gouge layer. The PSZ differs from other ancient slip zones in that it has not been affected by any later compaction or deformation (veins, fractures, or shear zones). The PSZ at 1,136 m does not show evidence of melting [*Boullier et al.*, 2009].

[6] The lower Pliocene Chinshui Formation (also called the Chinshui Shale) consists of alternating siltstones and ~10-cm-thick sandstones. Minerals in the siltstones are quartz, clays, and accessory minerals (feldspar, calcite) [*Isaacs et al.*, 2007]. Clay minerals consist of an assemblage of illite, chlorite, and kaolinite with accessory smectite [*Kuo et al.*, 2009]. Organic matter is present at a concentration of ~1% in the sediments, but its quantity is less than 0.7% in the fault zone [*Ikehara et al.*, 2007]. Iron sulfides are common in the undeformed and deformed sediments [*Boullier et al.*, 2009]. The Chinshui siltstones are unmetamorphosed with a recorded peak temperature due to modest burial of ~120°C based on vitrinite reflectance [*Sakaguchi et al.*, 2007].

3. Sampling and Methods

[7] For this study, we sampled the Chinshui Formation in TCDP Hole B across the ~20-cm-thick

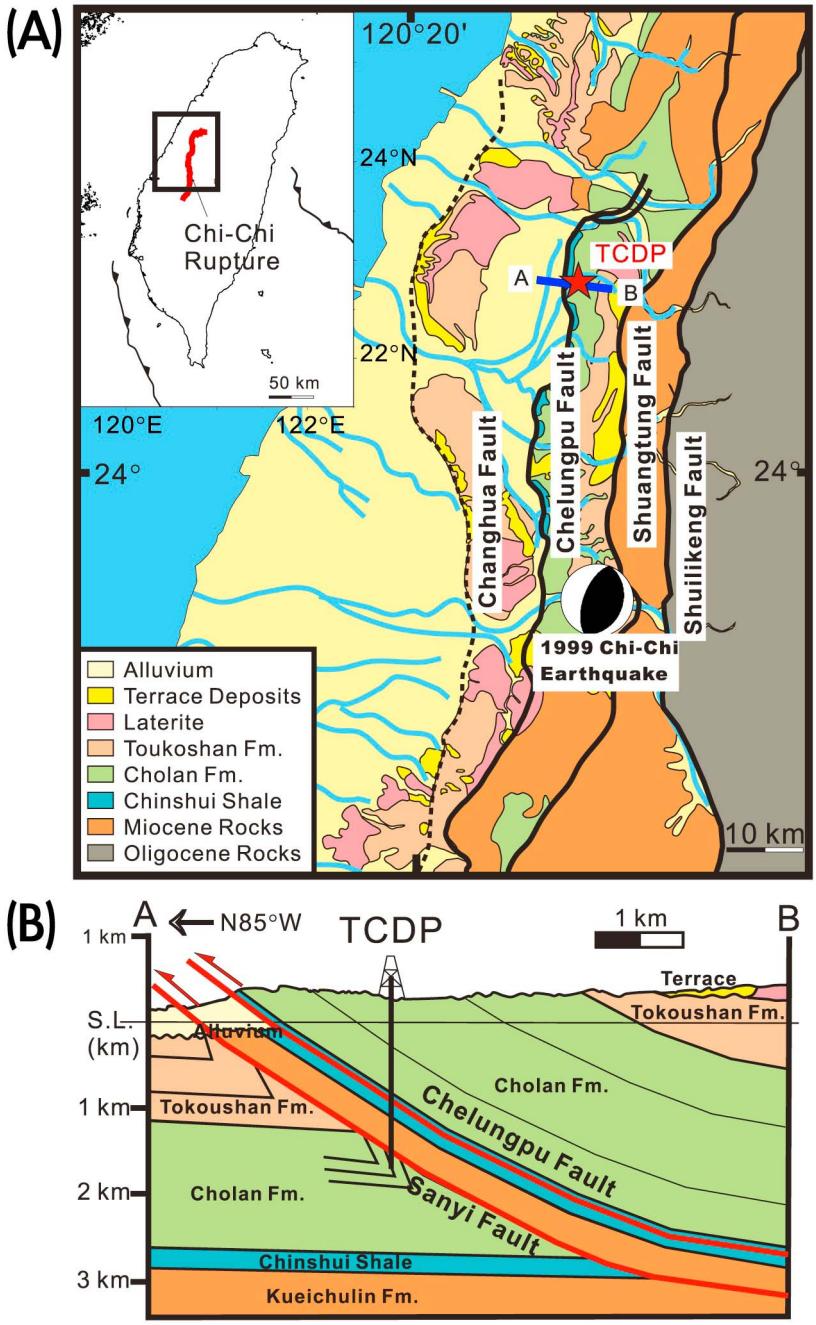

Figure 1. Geological setting of the TCDP borehole (modified from *Yeh et al.* [2007]). (a) Schematic geological map of western Taiwan with the location of the TCDP site (red star, 120.73916°E, 24.20083°N) on the northern part of the Chelungpu fault. The focal mechanism of the Chi-Chi main shock is located at the hypocenter of the 1999 Chi-Chi earthquake (128.81°E, 23.86°N). (b) Geological cross-section through the TCDP site. The Chelungpu fault is located within the Chinshui Formation.

fault zone (from 1,136.22 m to 1,136.43 m) together with wall rocks at different depths (Figures 2a and 2b; samples are listed in Table 1). In addition, we analyzed ten (2.5 cm × 2 cm) polished thin sections that were cut perpendicular to bedding within the fault plane (samples 1 to 10, Figure 2c) that were thoroughly described by *Boullier et al.* [2009]. These sections contain the boundaries between the gouge, the hanging wall, and the footwall deformed sediments. The deformed sediments were initially labeled 'gray gouge' principally because of their color [*Hirono*

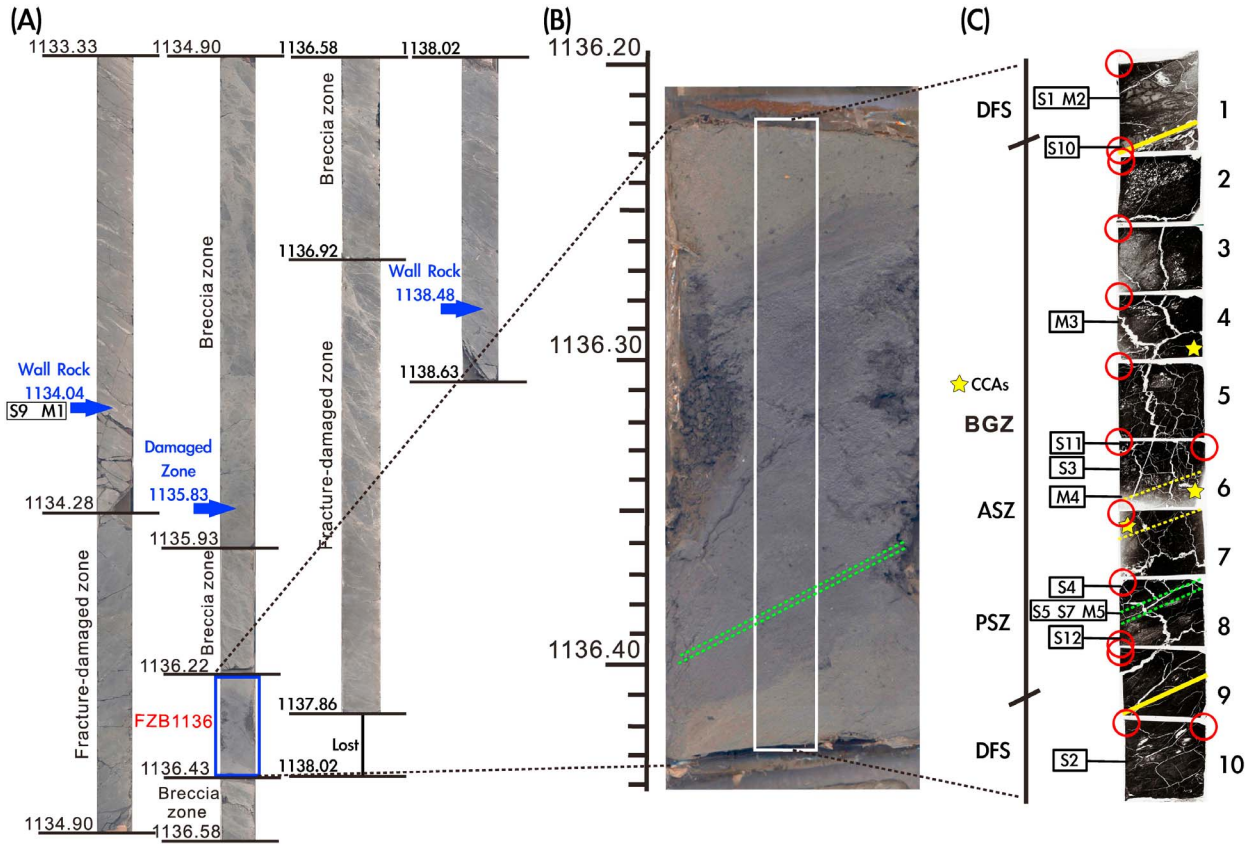

Figure 2. Images of the cores and samples from TCDP Hole B. (a) Half-core image for the depth interval from 1,133.33 to 1,138.63 m. The blue arrows and frame indicate the sample locations. (b) Half-core image of the FZB1136 fault zone at a depth of 1,136.22∼1,136.43 m; the white frame corresponds to the locations of polished sections. The green dashed line frames the Chi-Chi principal slip zone (PSZ) [*Boullier et al.*, 2009]. (c) Collage of SEM images from the polished sections. Red circles indicate sample positions for TXM analysis. The yellow lines are the boundaries between deformed sediments (DFS) and the gouge zone (BGZ). The yellow stars indicate clay-clast aggregates (CCAs [see *Boullier et al.*, 2009]). The double yellow dashed line is an ancient slip zone (ASZ) and the double green dashed line is the Chi-Chi PSZ [after *Boullier et al.*, 2009].

et al., 2007a]. However, within the 'gray gouge', bedding is preserved and thus the 'gray gouge' cannot be genetically related to gouge formation. To avoid confusion, we abandon the name 'gray gouge' in favor of 'deformed sediments' and we call gouge the 'black gouge' horizon. The ∼16-cm-thick gouge, which is surrounded by deformed sediments, constitutes a horizon of gouges where the bedding or other sedimentary structures are no longer preserved. Some gouges are reworked and are interpreted as ancient slip zones [*Boullier et al.*, 2009]. A 3-mm-thick level of gouge in thin section 8 (Figure 2c) is not reworked and consists of alternating clay-rich and clast-rich layers. *Boullier et al.* [2009] proposed that this slip zone was generated during the 1999 Chi-Chi event. Hereafter, it is referred to as the PSZ. From the 10 thin sections, we made scanning electron microscope (SEM) observations coupled with energy dispersive spectrometry (EDS) measurements and reflected-light polarizing microscope observations. We also made transmission X-ray microscopy (TXM) observations on 17 polished thick sections from the working section of TCDP Hole B core (Table 1). From these polished thick sections, we cut a few millimeter-long pieces and impregnated them with resin. Then, we cut each section into ∼15-μm-thick samples for TXM observation. We obtained fourteen 15-μm-thick samples from the fault zone, and three from the two parts of the hanging wall and footwall deformed sediments (Figure 2a and Table 1). For magnetic property measurements, we sampled hundreds of milligrams of rock powder within the ∼20-cm-thick fault zone, including deformed sediments and gouge.

Table 1. Sample Depths and Measurements Made in This Study[a]

Depth (m)	Location	Number	Measurements
1134.04	hanging wall rock	S9 M1	MPMS, FORC, TXM
1135.83	damaged zone		TXM, RFM
1136.22	deformed sediment	S1 M2	TXM, RFM, SEM, MPMS, FORC
1136.25	black gouge	S10	TXM, RFM, SEM
1136.27	black gouge		TXM, RFM
1136.29	black gouge	M3	TXM, RFM, SEM, MPMS, FORC
1136.31	black gouge		TXM, RFM
1136.33	black gouge	S3 S11	TXM, RFM, SEM
1136.35	ASZ	M4	TXM, RFM, SEM, MPMS, FORC
1136.37	black gouge	S4	TXM, RFM, SEM
1136.38	PSZ	S5 S7 M5	TXM, SEM, RFM, MPMS, FORC
1136.39	black gouge	S12	TXM, RFM, SEM
1136.41	deformed sediment		TXM, RFM, SEM
1138.48	footwall rock	S2	TXM

[a]FORC: First-order reversal curve, MPMS: Magnetic property measurement system, RFM: Reflected-light microscope, SEM: Scanning electron microscope, TXM: Transmission X-ray microscope.

[8] We used a LEO Stereoscan 440 SEM equipped with EDS (Analyzer EDX KEVEX SYGMA) for elemental analysis. The SEM was operated at 15 keV with 4 nA current. For TXM observation, we used the BL01B Beamline with 60 nm tomographic resolution at the National Synchrotron Radiation Research Center (NSRRC), Taiwan [*Yin et al.*, 2006; *Song et al.*, 2007b]. A superconducting wavelength shifter source provides a measured photon flux of 4.5×10^{11} photons/s/0.1% bw in the energy range 5–20 keV. X-rays generated by a wavelength shifter are primarily focused at a charge-coupled detector by a toroidal focusing mirror with a focal ratio of nearly 1:1. A double crystal monochromator that exploits a pair of Ge (111) crystals selects X-rays of energy 8–11 keV. After the focusing mirror and double crystal monochromator, a capillary condenser further shapes the X-ray beam. The condenser intercepts the impinging X-rays and further focuses them onto the sample. The image of the sample is magnified with a zone plate. The field of view of the image is $15 \times 15\ \mu m^2$ for the first-order diffraction mode of the zone plate. The phase term can be retrieved by the Zernike's phase contrast method for imaging light materials. The phase ring positioned at the back focal plane of the zone plate results in a recording of the phase contrast images at the detector. By acquiring a series of two-dimensional (2-D) images with the sample rotated stepwise, three-dimensional (3-D) tomography data sets are reconstructed from 141 images from $-70°$ to $+70°$. We scanned each sample over an area of 2700 μm^2.

[9] We also conducted a non-destructive magnetic investigation at room temperature (300 K) and at low temperature (10 to 300 K) to characterize the magnetic mineral assemblage in the deformed sediments and gouge in the Chi-Chi fault zone. In a first set of experiments, we measured the low-temperature dependency of a saturation isothermal remanent magnetization (SIRM) using a Quantum Designs Magnetic Property Measurement System (MPMS) XL5 EverCool system at the Institute de Physique du Globe de Paris (IPGP), France. To impart an SIRM, a magnetic field of 2.5 T was applied, either at room temperature (RT-SIRM at 300 K) or at low temperature (LT-SIRM at 10 K). We monitored successively the cooling and the warming demagnetization curves of the RT-SIRM and the LT-SIRM. We refer to warming curves of LT-SIRM as ZFC (zero field cooled). During cooling of the RT-SIRM, a positive magnetic field of 5 μT ($\sim$1/10 of the Earth's magnetic field) was applied to enable detection of a potential Néel transition. For samples M3, M4, and M5 (Table 1), we cycled the RT-SIRM during cooling and warming (cycling RT-SIRM). For this procedure, we removed the 5 μT magnetic field, and the residual magnetic field in the MPMS was <0.1 μT. We measured $\sim$400 mg of rock powder sealed in a gel-cap. In a second set of experiments, we measured first-order reversal curves (FORCs) [*Pike et al.*, 1999; *Roberts et al.*, 2000] using a Princeton Measurement Corporation vibrating sample magnetometer located at the Institute for Rock Magnetism (Minneapolis, USA). We measured FORCs using an averaging time of 0.5 s and processed the data using the FORCinel software [*Harrison and Feinberg*, 2008].

4. Results

4.1. Reflected-Light Polarizing Microscopy

[10] Inspection of thin sections using reflected-light polarizing microscopy indicates the presence of numerous framboids in the undeformed and deformed sediments. Complete extinction is observed for most of the framboids under polarized reflected-light, which suggests that they are isotropic minerals. The number of framboids decreases considerably from the deformed sediments to the gouge, where only a few reflective minerals (<25 μm) are observed. We

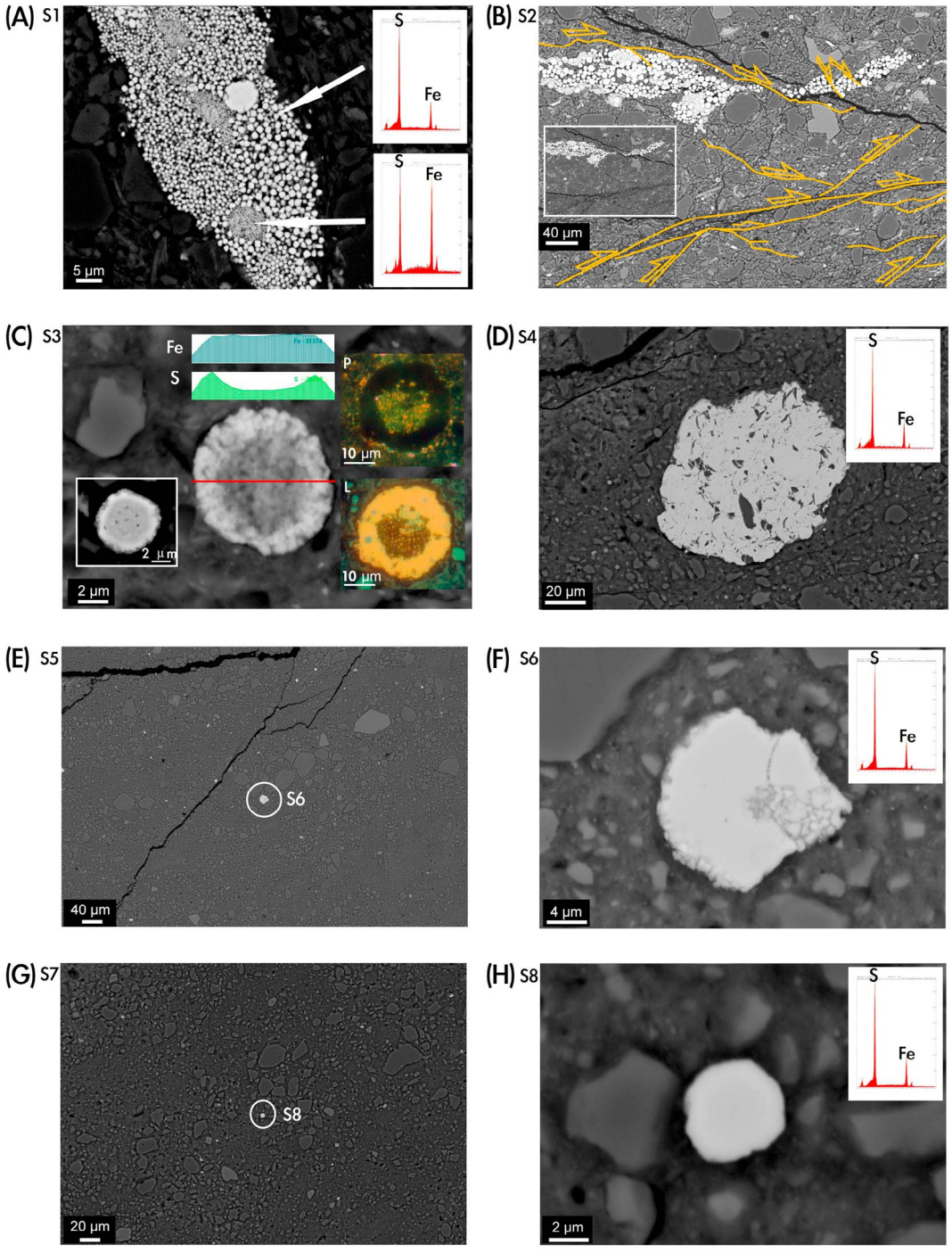

Figure 3. Backscattered SEM images with EDS results. (a) Large iron sulfide aggregates that contain framboidal pyrite (FeS_2) within the deformed sediments (S1 in Figure 2c). Some parts of the aggregate are greigite (Fe_3S_4). (b) Large iron sulfide aggregates that contain framboidal pyrite with micro-fractures and shears in the deformed sediments (S2 in Figure 2c). (c) Pyrite grain in the gouge (S3 in Figure 2c). The framboidal FeS core (pyrrhotite, which is a replacement of a framboidal pyrite) has an FeS_2 rim. The photos on the right were obtained using reflected-light microscopy (P: polarized reflected; L: light reflected); pyrite is dark and pyrrhotite is light under polarized light. (d) Large cluster of pyrite grains mixed with quartz (S4 in Figure 2c). (e) Small pyrite grains (bright backscattered grains, smaller than 5 μm, one is $\sim$20 μm) and quartz grains within the Chi-Chi PSZ (S8 in Figure 2c). (f) Detail of Figure 3e: fractured pyrite grain within the PSZ (S8 in Figure 2c). (g) Image of the Chi-Chi PSZ (S8 in Figure 2c). (h) Pyrite grain (3 μm) within the Chi-Chi PSZ (S8 in Figure 2c).

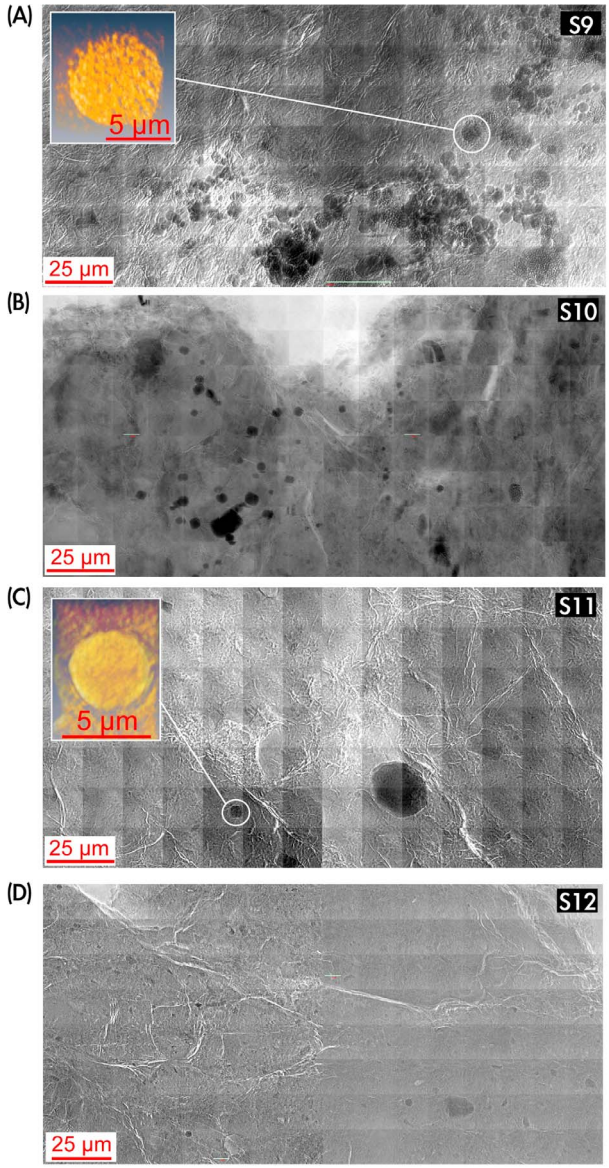

Figure 4. 2-D and 3-D images acquired for TXM observations. (a) Sediment at a depth of 1,134.04 m in TCDP hole B (M1 in Figure 2a). (b) Deformed sediment at a depth of 1,136.25 m (S10 in Figure 2c). (c) Gouge at a depth of 1,136.33 m (S11 in Figure 2c). (d) Gouge close to the PSZ at a depth of 1,136.38 m (S12 in Figure 2c).

did not observe magnetic minerals such as magnetite at the >1 μm scale.

4.2. SEM Observations

[11] In the deformed sediments close to the gouge, as well as in sediments from the hanging wall and footwall, numerous large iron sulfide aggregates include framboids of various sizes (1–5 μm) (Figure 3a). EDS analysis reveals that euhedral crystals within the framboids consist of pyrite (FeS_2). The size of pyrite crystals (~1 μm) is homogenous within framboids (Figure 3a). Isolated euhedral pyrite grains, with variable sizes, are also observed. Small framboids (~5 μm) consist of aggregates of ~100 nm iron monosulfide grains (FeS) (Figure 3a). FeS framboids are commonly observed from similar sediments in Taiwan and elsewhere and are interpreted as greigite (Fe_3S_4) framboids [*Jiang et al.*, 2001; *Roberts and Weaver*, 2005; *Rowan and Roberts*, 2006]. In deformed sediments close to the gouge, some iron sulfide aggregates have been dismembered by shearing (Figure 3b). From the pattern of shear planes, we identified a sense of shear that is consistent with the thrust orientation on the Chelungpu fault (Figure 3b).

[12] In the gouge (thin sections 2 to 9), we observed framboids of two types. Some framboids, with diameter of 5 to ~25 μm, have a FeS core surrounded by a 1~10 μm FeS_2 rim (Figure 3c). Under reflected-light microscopy, the core remains bright and the rim is black (Figure 3c, inset). This observation suggests that the FeS core is not cubic, which excludes the possibility that it is greigite. The second type of framboid is observed 1 mm from the PSZ (thin section 8). It consists of ~100 μm clusters of irregular-shaped pyrite crystals (Figure 3d). This resembles intensely deformed overgrown sedimentary sulfides. Within the 1999 Chi-Chi PSZ (thin section 8), we never observed framboids. Instead, small overgrown sulfide aggregates (<25 μm) are identified (Figure 3h). We also observed fine (<3 μm) pyrite grains scattered within the quartz and clay matrix (Figures 3g and 3h).

4.3. Transmission X-Ray Microscopy

[13] TXM provides three-dimensional (3-D) images of framboids that complement our two-dimensional (2-D) SEM and reflected-light microscopy observations. Within hanging wall (at a depth of 1,133.04 m) sediments, footwall (1,138.48 m) sediments, and deformed sediments (1,135.83 m) (Figure 2a), framboids are common (Figure 4a). Framboids are generally grouped in high concentrations in some parts of siltstones. This is probably a result of remineralization of large pieces of organic matter during early diagenesis [*Roberts and Weaver*, 2005]. Typically, the diameter of the framboids is larger than 10 μm, and the grain size of each pyrite crystal within the framboids is close to 1 μm.

[14] At a depth of 1,136.24 m in the borehole (thin section 2), a ~1-cm-thick layer of foliated gouge was identified by *Boullier et al.* [2009] (Figure 2c). There, TXM observations reveal the occurrence of numerous framboids together with dense spherical or cubic minerals (Figure 4b). The framboids are not aggregates and are scattered throughout the gouge. Within the gouge and near the 1999 Chi-Chi PSZ (Figures 4c and 4d), framboidal clusters are not observed. Instead, we observed 5 to 25 μm individual spherical-like mineral aggregates (Figure 4c) that probably correspond to the pyrite that we described in the gouge using SEM (Figures 3c and 3d).

4.4. Magnetic Properties

[15] Magnetic properties are comparable for the undeformed sediments (sample M1) and deformed sediments (sample M2) (Figures 5a and 5b). A Verwey transition at 120 K is detected in RT-SIRM demagnetization curves (see derivatives in insets in Figure 5) and in ZFC demagnetization curves. The Verwey transition indicates the occurrence of stoichiometric magnetite [*Özdemir and Dunlop*, 1999]. An additional magnetic transition is detected near 35 K for both ZFC and RT-SIRM demagnetization curves. This ~35 K transition is marked by a drop of one to two orders of magnitude of the LT-SIRM. The ~35 K transition is less evident in RT-SIRM demagnetization curves, with a break in slope at about 80 K followed by an enhancement of remanence (Figures 5a and 5b; see derivative). This behavior is similar to the P-behavior described by *Aubourg and Pozzi* [2010] and *Kars et al.* [2011]. The nature of P-behavior will be discussed later. We calculated the maximum concentration of magnetite by assuming that only magnetite contributes to the RT-SIRM at room temperature (300 K). The RT-SIRM at 300 K is less than 10^{-3} Am^2/kg for the different sediments that we measured. Taking the SIRM of magnetite as ~10 Am^2/kg [*Maher et al.*, 1999], we infer a maximum concentration of magnetite of 100 ppmv (concentration in parts per million by volume = $1 \times 10^6 \times$ RT-SIRM/$SIRM_{magnetite}$). FORC diagrams are noisy due to the small concentration of ferrimagnetic grains with respect to the paramagnetic contribution (Figures 5f and 5g), so high values of the smoothing factor (SF) were needed. The FORC diagrams are consistent with a distribution of weakly interacting single domain to superparamagnetic (SP) particles [e.g., *Pike et al.*, 2001; *Rowan and Roberts*, 2006].

[16] Gouge samples M3–M5 (Table 1) have different magnetic properties (Figures 5c–5e). From 300 K to 150 K, there is a regular increase of up to ~10% of the RT-SIRM. This increase is diagnostic of goethite (α-FeOOH) [*Dekkers*, 1989; *Maher et al.*, 1999; *Liu et al.*, 2006]. To check for the presence of goethite, we imparted a RT-SIRM at 300 K, and warmed it up to 400 K (Figure 6), which is close to Néel temperature of goethite (120°C [e.g., *Özdemir and Dunlop*, 1996]). About ~50% of the RT-SIRM is then lost at 400 K, which indicates that goethite contributes a large part of the artificial remanence. In the host sediments, by comparison, the increase of RT-SIRM from 300 K to 150 K is limited to 1 to 2% and the drop from 300 K to 400 K is less than 25%. In the gouge, the Verwey transition is much less pronounced and is observed only during cooling of the RT-SIRM (Figures 5d and 5e). The most notable difference is observed near 35 K. The ZFC curves do not undergo the one to two order magnitude remanence decrease at 35 K that is observed in host rock sediments. In addition, there is no P-behavior during cooling of the RT-SIRM. Instead, a ~35 K transition is characterized by a remanence drop despite application of a +5 μT magnetic field in the MPMS. This transition is similar to the magnetic transition for >1 μm pyrrhotite [*Dekkers et al.*, 1989; *Rochette et al.*, 1990]. According to *Dekkers et al.* [1989], the degree of reversibility of this transition is an indication of grain size. When cycling the RT-SIRM for sample M5 (Figure 7), we observed a reversible magnetic transition at 35 K, which indicates that pyrrhotite is fine-grained and close to 1 μm in size (h/c ratio 0.96). We calculated the maximum concentrations of goethite, pyrrhotite, and magnetite in the studied samples. At room temperature, the RT-SIRM is $<10^{-2}$ Am^2/kg for the different measured gouges. We assume that the contribution of goethite is about half of this value. Taking the SIRM of goethite as 0.05 Am^2/kg [*Maher et al.*, 1999], we obtain a maximum concentration of several percent goethite (RT-SIRM/$SIRM_{goethite}$). Assuming that the other half of the remanence is carried by pyrrhotite or magnetite, and assuming the SIRM of pyrrhotite as ~4.5 Am^2/kg and of magnetite as ~10 Am^2/kg [*Maher et al.*, 1999], we obtain a maximum concentration of pyrrhotite of less than 0.1% (concentration% = $100 \times$ RT-SIRM/$2SIRM_{pyrrhotite}$) and a maximum concentration of magnetite of less than 500 ppmv (concentration ppmv = $1 \times 10^6 \times$ RT-SIRM/$2SIRM_{magnetite}$). This suggests that there is an enhanced concentration of ferrimagnetic minerals in the gouge. FORC diagrams for gouge (M3) and PSZ (M5) have a significant high-coercivity contribution (Figures 5h and 5i). A coercivity peak at

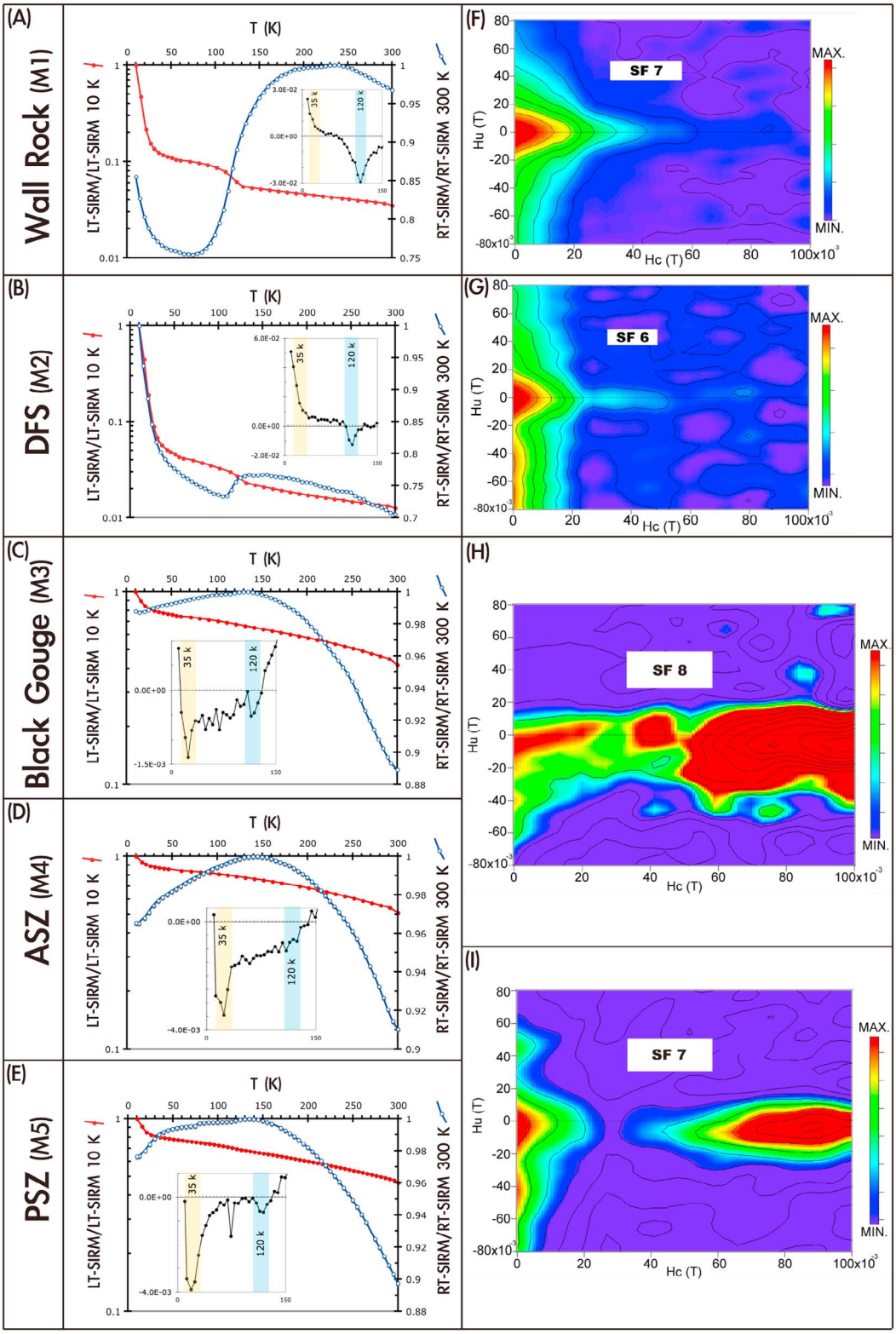

Figure 5. Low temperature magnetic measurements (inset: relative values of RT-SIRM) from 10 to 300 K and FORC diagrams. (a) Wall rock sample (M1 in Figure 2a). (b) Deformed sediment sample (M2 in Figure 2c). (c) Gouge sample (M3 in Figure 2c). (d) ASZ sample (M4 in Figure 2c). (e) PSZ sample (M5 in Figure 2c). (f) FORC diagram for wall rock sample (field 0–100 mT). (g) FORC diagram for deformed sediment sample (field 0–100 mT). (h and i) FORC diagrams for samples from fault gouge (field 0–100 mT).

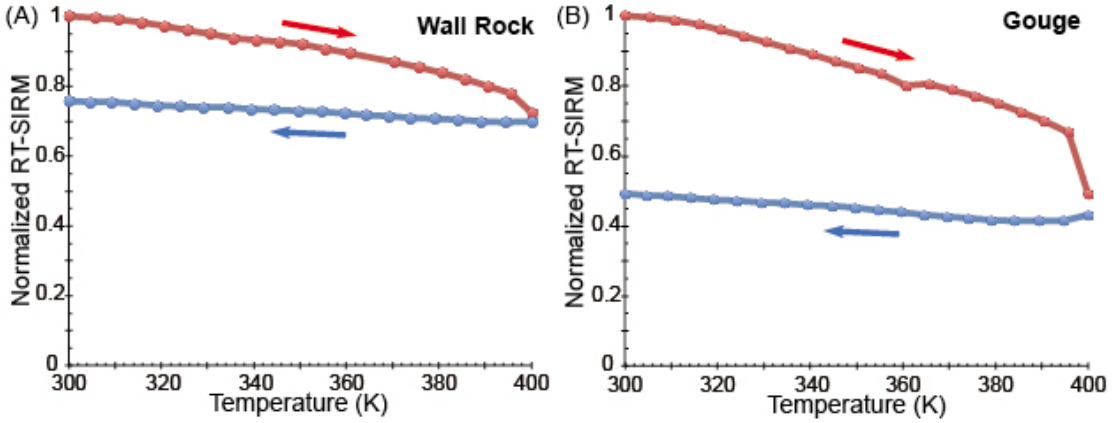

Figure 6. Warming-cooling RT-SIRM cycle from 300 to 400 K (127°C), which is close to the Néel temperature of goethite (120°C). (a) For a wall rock sample, less than 25% of the RT-SIRM is lost at 400 K. (b) For a gouge sample, about ~50% of the RT-SIRM is lost at 400 K. This indicates neoformation of a significant concentration of goethite in the fault gouge.

90 mT is consistent with the presence of magnetically interacting pyrrhotite [*Wehland et al.*, 2005; *Roberts et al.*, 2006]. Although goethite is identified using low-temperature remanence properties, we did not observe evidence of high-coercivities up to 500 mT in the FORC diagrams (data are not shown). We infer that the coercivity of this goethite is too high to contribute to the FORC distribution. *Rochette et al.* [2005] showed that natural goethite may not saturate even at fields up to 57 T.

5. Discussion

5.1. Iron Sulfides

[17] Iron sulfide minerals are common in organic matter rich sedimentary rocks [*Reimer*, 1984; *Tribovillard et al.*, 2002; *MacLean et al.*, 2008]. This is particularly true within Plio-Pleistocene sediments from Taiwan [*Horng et al.*, 1992, 1998; *Jiang et al.*, 2001] and within the Chinshui Formation, as confirmed by our observations. In these sediments, the iron sulfides typically form as framboids (Figures 3a, 3b, and 4a), but they can also appear as individual euhedral crystals. TXM inspection indicates that the framboids are not randomly scattered but are grouped as packs of tens of framboids in the sediments (Figures 3a, 3b, and 4a). SEM observations coupled with EDS analyses indicate that the framboids consist essentially of pyrite aggregates. However, small framboids (<0.1 μm) have an 'FeS' composition, and are likely greigite (Fe_3S_4). Greigite often forms during early [*Rowan et al.*, 2009] or late [*Roberts and Weaver*, 2005] diagenesis and is probably preserved in the unmetamorphosed Chinshui Formation. In deformed sediments, the only form of alteration of pyrite that we observed is the development of shear planes (Figure 3b). This is the first type of alteration of framboids that we detected in the deformed sediments. In the gouge, all micro-scale observations confirm the absence of well-preserved framboids.

[18] The pyrite content decreases drastically from the host sediments to the gouge. *Hirono et al.* [2007b] and *Ishikawa et al.* [2008] reported an

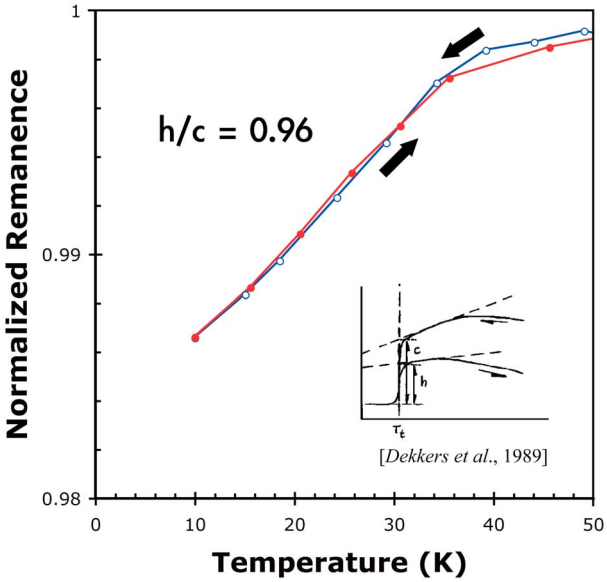

Figure 7. Cooling–warming RT-SIRM cycle from 10 to 50 K. A reversible magnetic transition at 35 K for the PSZ sample indicates that pyrrhotite is fine-grained and close to 1 μm in size (h/c ratio = 0.96) [see *Dekkers et al.*, 1989].

enhanced abundance of SO_4^{2-} in the gouge zone and related it to pyrite dissolution. Pyrite dissolution would release sulfate and would lower the pH of the immediately surrounding sediment [*Roberts and Weaver*, 2005]. Low pH conditions in turn would favor dissolution of carbonate minerals. This could be an alternative explanation for the low inorganic carbon content in the gouge [*Hirono et al.*, 2008; *Hamada et al.*, 2009; *Mishima et al.*, 2009].

[19] *Hirono et al.* [2008] reported a lack of pyrite in the gouge based on X-ray diffraction spectroscopy. Our observations contradict this view. In the gouge, we observe: 1) unusual small framboids (<25 μm) with FeS_2 as a rim and FeS as a core (Figure 3c), 2) detrital pyrite with irregular shapes (Figures 3d and 3f), and 3) individual <2 μm pyrite grains (Figure 3g). Individual pyrite grains are observed within the whole gouge, including the Chi-Chi PSZ (Figures 3e–3h). However, framboids have not been observed in the Chi-Chi PSZ.

[20] For the first time, we identified pyrrhotite in the gouge. This is based on the drop in remanence at ~35 K in the RT-SIRM demagnetization curves (Figure 7) which is a diagnostic signature of >1 μm pyrrhotite [*Dekkers et al.*, 1989; *Rochette et al.*, 1990]. The quasi-reversible path of the pyrrhotite transition indicates that the size of pyrrhotite grains is close to 1 μm [*Dekkers et al.*, 1989]. The distribution of coercivities around ~90 mT (Figures 5h and 5i) suggests that strongly interacting pyrrhotite dominates the magnetic assemblage of the gouge [*Wehland et al.*, 2005; *Roberts et al.*, 2006]. Our magnetic observations along with SEM observations reveal the occurrence of unusual framboids with rims of FeS_2 (pyrite) and cores of FeS (Figure 3c). The FeS phase included in framboids is likely pyrrhotite, which is detected magnetically, because it has grain sizes between 0.5 and 1 μm and is not cubic (Figure 3c). In addition, the strong magnetic interactions suggested by FORC diagrams can be explained by the tight grouping of pyrrhotite minerals enclosed in framboids. We never detected coarser >1 μm pyrrhotite in the Chinshui siltstones. Additional low-temperature magnetic experiments performed by *Humbert et al.* [2012] confirm our observations. We therefore argue that the coarser >1 μm pyrrhotite is not derived from the host rocks and that it was neoformed in the fault gouge.

[21] The preservation of iron sulfides like pyrite and the neoformation of pyrrhotite in the fault gouge are consistent with several observations. First, iron sulfide neoformation attests to a reducing environment in the gouge. This is in agreement with geochemical observations in the gouge from FZB1136 [*Ishikawa et al.*, 2008]. Second, the association of pyrite and pyrrhotite may imply heating and cooling during co-seismic and post-seismic processes. We assume that pyrrhotite formation is related to alteration of pyrite grains. *Chin et al.* [2005] observed that mechanical milling of pyrite under CO_2-rich conditions triggered pyrrhotite formation. This process is feasible in a gouge where milling is a common process. However, we infer the presence of large pyrrhotite grains (~1 μm) grains in the FZB1136 gouge, which is supported by direct observations of framboid relics that have not been completely crushed (Figure 3c). Therefore, we conclude that an additional process occurred. *Wang et al.* [2008] demonstrated that oxidation of pyrite to pyrrhotite or hematite can occur during short-term exposure to temperatures up to 700°C (heating rate: 11°C/minute). With a similar heating rate, *Bhargava et al.* [2009] observed that heating of pyrite yields pyrrhotite at 500°C under inert conditions (pure N_2 or Ar gas). This is consistent with the heating experiments of *Mayoral et al.* [2002] at 500°C with a higher heating rate (80°C/minute). When extrapolating these experimental results to our study, we suggest that elevated temperatures of >500°C in the gouge triggered pyrrhotite formation at the expense of pyrite. The gouge is a stack of numerous slip zones, and within each slip zone elevated temperatures are likely due to frictional processes [*Boullier et al.*, 2009]. Even if there is no evidence of melting in the FZB1136 gouge [*Hirono et al.*, 2008; *Boullier et al.*, 2009], temperatures above 500°C are nevertheless possible in parts of the gouge, including the 1999 Chi-Chi PSZ. Therefore, we suggest that pyrrhotite formed at temperatures >500°C associated with repeated earthquakes.

[22] A temperature above 350°C in the gouge has been proposed by several authors, based on geochemistry [*Ishikawa et al.*, 2008], carbonate alteration [*Hirono et al.*, 2008], vaporization of water during thermal pressurization [*Boullier et al.*, 2009], and formation of magnetic minerals [*Hirono et al.*, 2006; *Tanikawa et al.*, 2008; *Mishima et al.*, 2009]. *Ishikawa et al.* [2008] suggested that the chemical characteristics of the gouge were produced by interaction with co-seismic aqueous fluids derived from sediment pore waters with temperatures up to 350°C. We calculated Eh-pH diagrams using the Geochemist's Workbench software and considered the stability of pyrite and

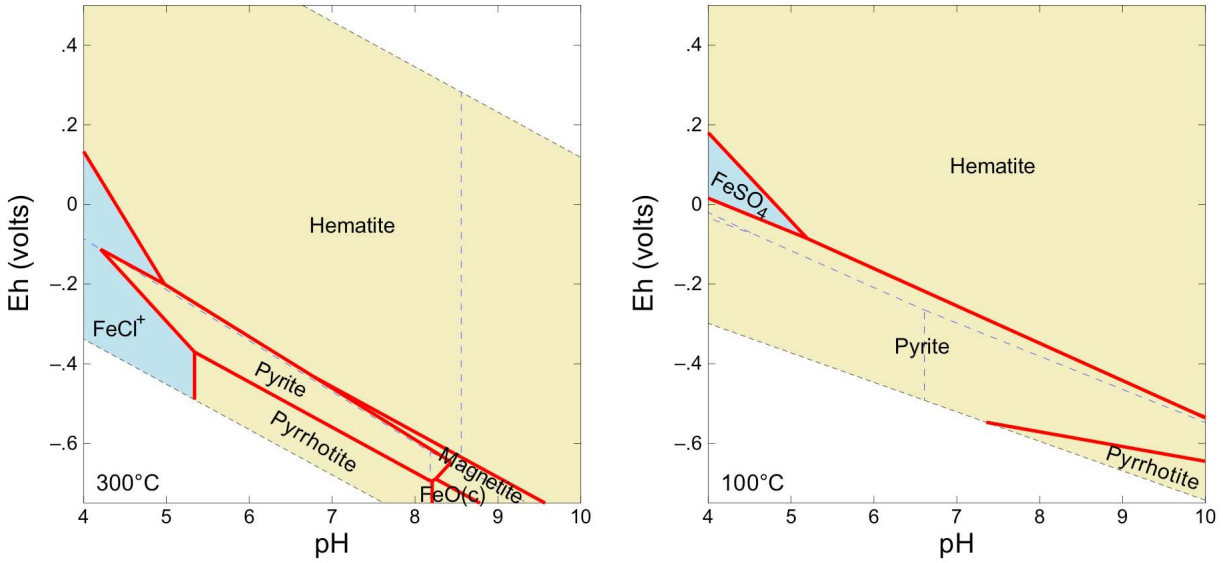

Figure 8. Eh-pH diagrams for fluid temperatures of 300°C and 100°C. The model parameters are: $a_{SO42-} = 10^{-2}$, $a_{Cl-} = 10^{-2}$, $a_{Fe2+} = 10^{-4}$ (higher iron concentration). The pressure used is 30 MPa, which is equivalent to lithostatic pressure at a depth of 1,100 m. Note that at higher temperatures the pyrrhotite field exists at strong reducing conditions in a pH range of 5.3–8.2. As temperature decreases, the pyrite field expands and pyrrhotite alters to pyrite.

pyrrhotite in an aqueous fluid within the gouge (Figure 8). The pyrite stability field increases from 300 to 100°C at lower Eh conditions. The gouge appears to have formed under anoxic conditions based on microbial observations at 1,000 m depth in TCDP core Hole A [*Wang et al.*, 2007]. We suggest that pyrite formed as a result of retrograde metamorphism. The presence of pyrite rims on pyrrhotite cores in the framboids (Figure 3c) supports the retrograde metamorphism hypothesis. Only pyrrhotite on the surface of framboids will be affected by retrograde metamorphism, and the core of pyrrhotite will be preserved. If correct, this suggests that most pyrite in the gouge (Figures 3e–3h) resulted from retrograde metamorphism during cooling of co-seismic fluids from above 350°C.

5.2. Magnetite

[23] Magnetite is present in the Chinshui Formation, and recognition of the Verwey transition (~120 K; Figure 5a) implies the occurrence of stoichiometric magnetite with a maximum concentration of 100 ppmv. *Mishima et al.* [2009] also reported a low concentration of magnetite in the Chinshui siltstones. The marked ~35 K magnetic transition observed from ZFC demagnetization curves (Figure 5), also observed by *Mishima et al.* [2009], could be explained by superparamagnetic (SP) grains, monoclinic pyrrhotite, siderite ($FeCO_3$), and rhodochrosite ($MnCO_3$) [*Housen et al.*, 1996; *Kars et al.*, 2011]. It is well known that magnetite nanoparticles carry a remanence at low temperature (typically 10 K), and that they lose this remanence on warming [*Hunt et al.*, 1995]. *Mishima et al.* [2009] attributed this 35 K transition to SP grains in the Chinshui Formation. Although we agree with *Mishima et al.* [2009], from the same samples we observed development of a magnetic transition with a break-in-slope at ~35 K on RT-SIRM demagnetization curves (Figure 5). *Aubourg and Pozzi* [2010] and *Kars et al.* [2011] observed the same behavior in unmetamorphosed claystones. They proposed that this magnetic transition, referred to as P-behavior, is due to a combination of a fine-grained pyrrhotite transition and an induced magnetization of unknown origin. We support this interpretation because of the strong similarity of low-temperature demagnetization curves (ZFC, RT-SIRM) of Chinshui Formation sedimentary rocks with those reported by *Aubourg and Pozzi* [2010] and *Kars et al.* [2011]. If correct, the presence of stoichiometric fine-grained magnetite and fine-grained pyrrhotite of the Chinshui Formation is diagnostic of modest burial below 5 km [*Aubourg and Pozzi*, 2010; *Abdelmalak et al.*, 2012]. This is consistent with a burial temperature of about 120°C, inferred from vitrinite reflectance data (R0~0.8%) [*Sakaguchi et al.*, 2007].

[24] The magnetic properties of gouge differ from those of the host sediments. In particular, we

observe a weakening of the Verwey transition (Figures 5c–5e), which suggests that magnetite is partially oxidized [*Özdemir et al.*, 1993; *Cui et al.*, 1994; *Özdemir et al.*, 2002]. The presence of co-seismic hot fluids in the gouge [*Ishikawa et al.*, 2008] constitutes a possible explanation for the partial alteration of magnetite, where magnetite could be oxidized to maghemite thereby causing weakening of the Verwey transition [*Özdemir et al.*, 1993; *Cui et al.*, 1994; *Özdemir et al.*, 2002]. The absence of a large remanence drop between 10 K and 40 K in the ZFC demagnetization curves (Figures 5a and 5b) implies that the grain size fraction of magnetite is essentially above the SP threshold size (∼20 nm). Paradoxically, ultrafine-grained magnetic minerals present in the Chinshui Formation do not exist in the gouge, where grain size reduction by a milling process is likely. We interpret that the ultrafine fraction is altered chemically during repeated earthquakes. *Aubourg and Pozzi* [2010] showed that moderate heating up to 250°C promotes drastic reduction of the 35 K magnetic transition. We suggest, therefore, that the increased temperature in the gouge alters the ultrafine-grained fraction of magnetic minerals.

[25] A fraction of magnetite could have been inherited from the Chinshui Formation. However, detrital magnetite is probably unlikely in sediments that have been extensively pyritized [*Rowan et al.*, 2009]. Magnetite can form at elevated temperatures, by precipitation from frictional melts as observed in natural pseudotachylites [*Ferré et al.*, 2005, 2012] or in experimental pseudotachylites [*Nakamura et al.*, 2002]. Similar to pyrrhotite, we suggest that some magnetite formed during repeated earthquakes within the gouge.

5.3. Goethite

[26] The evolution of remanence on heating and cooling (Figures 5c–5e) also suggests the occurrence of goethite (α-FeOOH) in the gouge. Recognition of goethite is important because it demonstrates the presence of fluid in the gouge. In a companion paper, we provided additional evidence for the occurrence of goethite [*Chou et al.*, 2012] and showed that the natural remanent magnetization in the gouge is carried essentially by goethite. We suggest that this magnetization record is contemporaneous with the 1999 Chi-Chi event. TXM tomography identified scattered 5 μm goethite grains within the gouge. The remanence and TXM observations led *Chou et al.* [2012] to propose that goethite formed from cooling of co-seismic fluids within the gouge. Low pH conditions associated with pyrite alteration would favor goethite formation [*Schwertmann and Murad*, 1983; *Murad and Rojik*, 2003]. In addition, *Nakamura and Nagahama* [2001] also observed 5 μm goethite in the Nojima fault gouge from Japan. We therefore suggest that study of goethite in fault gouge is important to detect evidence of co-seismic fluids and could be an indicator of thermal pressurization.

5.4. Implications for Identification of Earthquake Slip Zones

[27] In sediment-derived fault gouge, endothermic dehydration reactions and the phase change from liquid water to steam can efficiently buffer the temperature within a fault [*Brantut et al.*, 2011]. This is consistent with the scarcity of melts in sediment-derived fault gouge, as was observed in the FZB1136 gouge [*Boullier et al.*, 2009]. Generally, recognition of clay-clast aggregates (CCA) [*Boullier et al.*, 2009] is good evidence of thermal pressurization processes, and, in turn, as a signature of earthquakes [*Boutareaud et al.*, 2008]. Identification of neoformed minerals can be an alternative indicator of limited temperature elevation and fluid interaction. In this regard, we suggest that at the time of pyrrhotite formation in the FZB1136 gouge, this implies a temperature above 500°C. Similarly, we suggest that goethite formation is an indication of thermal pressurization processes. In fold-and-thrust belts, thrusts similar to the Chelungpu fault are common and likely developed within clay-rich rocks. If pyrrhotite and goethite exist in the gouge, and not in the host rocks, then it can be inferred that temperature enhancement took place and that fluids infiltrated the gouge.

6. Conclusions

[28] The 16-cm-thick gouge zone intersected in the TCDP drill holes is a product of repeated earthquakes, including the Chi-Chi earthquake (M_w 7.6, 1999), and has had a complex mechanical and thermal history. The wall rocks are made up of the Chinshui Formation, which contains several percent pyrite. The magnetic mineral assemblage of this formation is typical of unmetamorphosed sediments and consists essentially of nanometric stoichiometric magnetite. Micro-scale observations indicate that the concentration of pyrite framboids decreases considerably from the wall rock into the gouge. Pyrite alteration would cause a lowering of pH, and, in turn, would promote carbonate mineral dissolution. Beside pyrite alteration, we identify for the first time the occurrence of micrometric pyrrhotite in the

fault gouge. The pyrrhotite likely formed at high temperatures (>500°C) at the expense of pyrite. Magnetite, which is also present in the gouge, is partially altered. We propose that pyrrhotite and some of the magnetite formed at elevated temperatures during frictional heating along the slip zones. The total concentration of pyrrhotite and magnetite is therefore a result of numerous earthquakes. In the gouge, we also identify neoformed goethite, which implies the presence of hot fluids (>350°C). On cooling, these hot fluids altered pyrrhotite into pyrite and magnetite into partially altered magnetite. Our results demonstrate that characterization of magnetic minerals provides a useful means of studying earthquake processes in faults.

Acknowledgments

[29] We thank the working group of TCDP for core drilling. The National Science Council of Taiwan under grants NSC 95-2745-M-002-001, NSC 96-2627-M-002-011 and NSC 97-2627-M-213-001 with a TEC contribution number supported this research. Yu-Min Chou was supported by an Eiffel excellence scholarship program (EGIDE, France) and the Graduate Student Study Abroad Program (NSC, Taiwan). We thank Guang-Chian Yin of NSRRC for maintenance of the TXM and Keng S. Liang of NSRRC for supporting this project. The MPMS XL5 EverCool used in this study was financed by the Conseil Régional d'Ile-de-France (I-06-206/R), INSU-CNRS, IPGP, and ANR. We also thank Christophe Nevado (Geosciences Montpellier) for making polished thin sections of difficult gouge material, and Olivier Romeyer (Plate-Forme d'Analyze Structurale, Université de Savoie at Chambéry) for his technical assistance when using the SEM. L.-W. Kuo, P. Robion, C. David, L. Louis, and F. Humbert are thanked for constructive discussions. This paper benefited from constructive reviews by A. P. Roberts and J. W. Geissman.

References

Abdelmalak, M. M., C. Aubourg, L. Geoffroy, and F. Laggoun-Deffarge (2012), A new oil window indicator? The magnetic assemblage of claystones from the Baffin Bay volcanic margin (Greenland), *AAPG Bull.*, *96*, 205–215, doi:10.1306/07121111008.

Aubourg, C., and J.-P. Pozzi (2010), Toward a new <250°C pyrrhotite-magnetite geothermometer for claystones, *Earth Planet. Sci. Lett.*, *294*, 47–57, doi:10.1016/j.epsl.2010.02.045.

Berner, R. A. (1984), Sedimentary pyrite formation: An update, *Geochim. Cosmochim. Acta*, *48*, 605–615, doi:10.1016/0016-7037(84)90089-9.

Bhargava, S. K., A. Garg, and N. D. Subasinghe (2009), In situ high-temperature phase transformation studies on pyrite, *Fuel*, *88*(6), 988–993, doi:10.1016/j.fuel.2008.12.005.

Boullier, A.-M., E.-C. Yeh, S. Boutareaud, S.-R. Song, and C.-H. Tsai (2009), Microscale anatomy of the 1999 Chi-Chi earthquake fault zone, *Geochem. Geophys. Geosyst.*, *10*, Q03016, doi:10.1029/2008GC002252.

Boutareaud, S. B., D.-G. Calugaru, R. Han, O. Fabbri, K. Mizoguchi, A. Tsutsumi, and T. Shimamoto (2008), Clay-clast aggregates: A new textural evidence for seismic fault sliding?, *Geophys. Res. Lett.*, *35*, L05302, doi:10.1029/2007GL032554.

Brantut, N., R. Han, T. Shimamoto, N. Findling, and A. Schubnel (2011), Fast slip with inhibited temperature rise due to mineral dehydration: Evidence from experiments on gypsum, *Geology*, *39*, 59–62, doi:10.1130/g31424.1.

Chen, Y.-G., W.-S. Chen, Y. Wang, P.-W. Lo, J.-C. Lee, and T.-K. Liu (2002), Geomorphic evidence for prior earthquakes: Lesson from the 1999 Chichi earthquake in central Taiwan, *Geology*, *30*, 171–174, doi:10.1130/0091-7613(2002)030<0171:GEFPEL>2.0.CO;2.

Chin, P. P., J. Ding, J. B. Yi, and B. H. Liu (2005), Synthesis of FeS_2 and FeS nanoparticles by high-energy mechanical milling and mechanochemical processing, *J. Alloys Compd.*, *390*, 255–260, doi:10.1016/j.jallcom.2004.07.053.

Chou, Y.-M., S.-R. Song, C. Aubourg, T.-Q. Lee, A.-M. Boullier, Y.-F. Song, E.-C. Yeh, L.-W. Kuo, and C.-Y. Wang (2012), An earthquake slip zone is a magnetic recorder, *Geology*, *40*, 551–554, doi:10.1130/G32864.1.

Craig, J. R., F. M. Vokes, and T. N. Solberg (1998), Pyrite: Physical and chemical textures, *Miner. Deposita*, *34*, 82–101, doi:10.1007/s001260050187.

Cui, Y., K. L. Verosub, and A. P. Roberts (1994), The effect of low temperature oxidation on large multi-domain magnetite, *Geophys. Res. Lett.*, *21*, 757–760, doi:10.1029/94GL00639.

Dekkers, M. J. (1989), Magnetic properties of natural goethite—II. TRM behaviour during thermal and alternating field demagnetization and low-temperature treatment, *Geophys. J. Int.*, *97*, 341–355, doi:10.1111/j.1365-246X.1989.tb00505.x.

Dekkers, M. J., J. L. Mattéi, G. Fillion, and P. Rochette (1989), Grain-size dependence of the magnetic behavior of pyrrhotite during its low-temperature transition at 34 K, *Geophys. Res. Lett.*, *16*, 855–858, doi:10.1029/GL016i008p00855.

Ferré, E. C., M. S. Zechmeister, J. W. Geissman, N. Mathana-Sekaran, and K. Kocak (2005), The origin of high magnetic remanence in fault pseudotachylites: Theoretical considerations and implication for coseismic electrical currents, *Tectonophysics*, *402*, 125–139, doi:10.1016/j.tecto.2005.01.008.

Ferré, E. C., J. W. Geissman, and M. S. Zechmeister (2012), Magnetic properties of fault pseudotachylytes in granites, *J. Geophys. Res.*, *117*, B01106, doi:10.1029/2011JB008762.

Fukuchi, T., K. Mizoguchi, and T. Shimamoto (2005), Ferrimagnetic resonance signal produced by frictional heating: A new indicator of paleoseismicity, *J. Geophys. Res.*, *110*, B12404, doi:10.1029/2004JB003485.

Hamada, Y., T. Hirono, W. Tanikawa, W. Soh, and S.-R. Song (2009), Energy taken up by co-seismic chemical reactions during a large earthquake: An example from the 1999 Taiwan Chi-Chi earthquake, *Geophys. Res. Lett.*, *36*, L06301, doi:10.1029/2008GL036772.

Harrison, R. J., and J. M. Feinberg (2008), FORCinel: An improved algorithm for calculating first-order reversal curve distributions using locally weighted regression smoothing, *Geochem. Geophys. Geosyst.*, *9*, Q05016, doi:10.1029/2008GC001987.

Hirono, T., et al. (2006), High magnetic susceptibility of fault gouge within Taiwan Chelungpu fault: Nondestructive continuous measurements of physical and chemical properties in fault rocks recovered from Hole B, TCDP, *Geophys. Res. Lett.*, *33*, L19311, doi:10.1029/2006GL027329.

Hirono, T., et al. (2007a), Nondestructive continuous physical property measurements of core samples recovered from hole B, Taiwan Chelungpu-Fault Drilling Project, *J. Geophys. Res.*, *112*, B07404, doi:10.1029/2006JB004738.

Hirono, T., et al. (2007b), A chemical kinetic approach to estimate dynamic shear stress during the 1999 Taiwan Chi-Chi earthquake, *Geophys. Res. Lett.*, *34*, L19308, doi:10.1029/2007GL030743.

Hirono, H., et al. (2008), Characterization of slip zone associated with the 1999 Taiwan Chi-Chi earthquake: X-ray CT image analyses and microstructural observations of the Taiwan Chelungpu fault, *Tectonophysics*, *449*, 63–84, doi:10.1016/j.tecto.2007.12.002.

Horng, C.-S., C. Laj, T.-Q. Lee, and J.-C. Chen (1992), Magnetic characteristics of sedimentary rocks from the Tsengwen-chi and Erhjen-chi sections in southwestern Taiwan, *Terr. Atmos. Oceanic Sci.*, *3*, 519–532.

Horng, C.-S., M. Torii, K.-S. Shea, and S.-J. Kao (1998), Inconsistent magnetic polarities between greigite- and pyrrhotite/magnetite-bearing marine sediments from the Tsailiao-chi section, southwestern Taiwan, *Earth Planet. Sci. Lett.*, *164*, 467–481, doi:10.1016/S0012-821X(98)00239-8.

Housen, B. A., S. K. Banerjee, and B. M. Moskowitz (1996), Low-temperature magnetic properties of siderite and magnetite in marine sediments, *Geophys. Res. Lett.*, *23*, 2843–2846, doi:10.1029/96GL01197.

Humbert, F., P. Robion, L. Louis, D. L. Bartier, B. A. Ledésert, and S.-R. Song (2012), Magnetic inference of in situ open microcracks in sandstone samples from the Taiwan Chelungpu Fault Drilling Project (TCDP), *J. Asian Earth Sci.*, *45*, 179–189, doi:10.1016/j.jseaes.2011.10.009.

Hunt, C. P., S. K. Banerjee, J. Han, P. A. Solheld, E. Oches, W.-W. Sun, and T. Liu (1995), Rock-magnetic proxies of climate change in the loess-palaeosol sequences of the western Loess Plateau of China, *Geophys. J. Int.*, *123*, 232–244, doi:10.1111/j.1365-246X.1995.tb06672.x.

Ikehara, M., et al. (2007), Low total and inorganic carbon contents within the Taiwan Chelungpu fault system, *Geochem. J.*, *41*, 391–396, doi:10.2343/geochemj.41.391.

Isaacs, A. J., J. P. Evans, S.-R. Song, and P. T. Kolesar (2007), Structural, mineralogical, and geochemical characterization of the Chelungpu thrust fault, Taiwan, *Terr. Atmos. Oceanic Sci.*, *18*, 183–221, doi:10.3319/TAO.2007.18.2.183(TCDP).

Ishikawa, T., et al. (2008), Coseismic fluid-rock interactions at high temperatures in the Chelungpu fault, *Nat. Geosci.*, *1*, 679–683, doi:10.1038/ngeo308.

Jiang, W.-T., C.-S. Horng, A. P. Roberts, and D. R. Peacor (2001), Contradictory magnetic polarities in sediments and variable timing of neoformation of authigenic greigite, *Earth Planet. Sci. Lett.*, *193*, 1–12, doi:10.1016/S0012-821X(01)00497-6.

Jovanović, D. (1989), Kinetics of thermal decomposition of pyrite in an inert atmosphere, *J. Therm. Anal. Calorim.*, *35*, 1483–1492, doi:10.1007/BF01912925.

Kano, Y., J. Mori, R. Fujio, H. Ito, T. Yanagidani, S. Nakao, and K.-F. Ma (2006), Heat signature on the Chelungpu fault associated with the 1999 Chi-Chi, Taiwan earthquake, *Geophys. Res. Lett.*, *33*, L14306, doi:10.1029/2006GL026733.

Kao, H., and W.-P. Chen (2000), The Chi-Chi earthquake sequence: Active, out-of-sequence thrust faulting in Taiwan, *Science*, *288*, 2346–2349, doi:10.1126/science.288.5475.2346.

Kars, M., C. Aubourg, and J.-P. Pozzi (2011), Low temperature magnetic behaviour near 35 K in unmetamorphosed claystones, *Geophys. J. Int.*, *186*, 1029–1035, doi:10.1111/j.1365-246X.2011.05121.x.

Kuo, L.-W., S.-R. Song, E.-C. Yeh, and H.-F. Chen (2009), Clay mineral anomalies in the fault zone of the Chelungpu Fault, Taiwan, and their implications, *Geophys. Res. Lett.*, *36*, L18306, doi:10.1029/2009GL039269.

Lambert, J., G. Simkovich, and P. Walker (1998), The kinetics and mechanism of the pyrite-to-pyrrhotite transformation, *Metall. Mater. Trans. B*, *29*, 385–396, doi:10.1007/s11663-998-0115-x.

Liu, Q., Y. Yu, J. Torrent, A. P. Roberts, Y. Pan, and R. Zhu (2006), Characteristic low-temperature magnetic properties of aluminous goethite [α-(Fe, Al)OOH] explained, *J. Geophys. Res.*, *111*, B12S34, doi:10.1029/2006JB004560.

Liu, Y., and Q. Liu (2004), Flotation separation of carbonate from sulfide minerals, I: Flotation of single minerals and mineral mixtures, *Miner. Eng.*, *17*, 855–863, doi:10.1016/j.mineng.2004.03.006.

Ma, K.-F., C.-T. Lee, Y.-B. Tsai, T.-C. Shin, and J. Mori (1999), The Chi-Chi, Taiwan earthquake: Large surface displacements on an inland thrust fault, *Eos Trans. AGU*, *80*(50), 605, doi:10.1029/99EO00405.

Ma, K.-F., E. E. Brodsky, J. Mori, C. Ji, T.-R. A. Song, and H. Kanamori (2003), Evidence for fault lubrication during the 1999 Chi-Chi, Taiwan, earthquake (Mw7.6), *Geophys. Res. Lett.*, *30*(5), 1244, doi:10.1029/2002GL015380.

Ma, K.-F., et al. (2006), Slip zone and energetics of a large earthquake from the Taiwan Chelungpu-fault Drilling Project, *Nature*, *444*, 473–476, doi:10.1038/nature05253.

MacLean, L. C. W., T. Tyliszczak, P. U. P. A. Gilbert, D. Zhou, T. J. Pray, T. C. Onstott, and G. Southam (2008), A high-resolution chemical and structural study of framboidal pyrite formed within a low-temperature bacterial biofilm, *Geobiology*, *6*, 471–480, doi:10.1111/j.1472-4669.2008.00174.x.

Maher, B. A., R. Thompson, and M. W. Hounslow (1999), Introduction, in *Quaternary Climates, Environments and Magnetism*, edited by B. A. Maher and R. Thompson, pp. 1–48, Cambridge Univ. Press, Cambridge, U. K.

Mayoral, M. C., M. T. Izquierdo, J. M. Andrés, and B. Rubio (2002), Mechanism of interaction of pyrite with hematite as simulation of slagging and fireside tube wastage in coal combustion, *Thermochim. Acta*, *390*, 103–111, doi:10.1016/S0040-6031(02)00075-8.

Mishima, T., T. Hirono, N. Nakamura, W. Tanikawa, W. Soh, and S.-R. Song (2009), Changes to magnetic minerals caused by frictional heating during the 1999 Taiwan Chi-Chi earthquake, *Earth Planets Space*, *61*, 797–801.

Murad, E., and P. Rojik (2003), Iron-rich precipitates in a mine drainage environment: Influence of pH on mineralogy, *Am. Mineral.*, *88*, 1915–1918.

Music, S., S. Popović, and M. Ristić (1992), Thermal decomposition of pyrite, *J. Radioanal. Nucl. Chem.*, *162*, 217–226, doi:10.1007/BF02035382.

Nakamura, N., and H. Nagahama (2001), Changes in magnetic and fractal properties of fractured granites near the Nojima Fault, Japan, *Isl. Arc*, *10*, 486–494, doi:10.1046/j.1440-1738.2001.00347.x.

Nakamura, N., T. Hirose, and G. J. Borradaile (2002), Laboratory verification of submicron magnetite production in pseudotachylytes: Relevance for paleointensity studies, *Earth Planet. Sci. Lett.*, *201*, 13–18, doi:10.1016/S0012-821X(02)00704-5.

Özdemir, Ö., and D. J. Dunlop (1996), Thermoremanence and Néel temperature of goethite, *Geophys. Res. Lett.*, *23*, 921–924, doi:10.1029/96GL00904.

Özdemir, Ö., and D. J. Dunlop (1999), Low-temperature properties of a single crystal of magnetite oriented along principal magnetic axes, *Earth Planet. Sci. Lett.*, *165*, 229–239, doi:10.1016/S0012-821X(98)00269-6.

Özdemir, Ö., D. J. Dunlop, and B. M. Moskowitz (1993), The effect of oxidation on the Verwey transition in magnetite, *Geophys. Res. Lett.*, *20*, 1671–1674, doi:10.1029/93GL01483.

Özdemir, Ö., D. J. Dunlop, and B. M. Moskowitz (2002), Changes in remanence, coercivity and domain state at low temperature in magnetite, *Earth Planet. Sci. Lett.*, *194*, 343–358, doi:10.1016/S0012-821X(01)00562-3.

Pelovski, Y., and V. Petkova (1999), Investigation on thermal decomposition of pyrite part I, *J. Therm. Anal. Calorim.*, *56*, 95–99, doi:10.1023/A:1010135425009.

Pike, C. R., A. P. Roberts, and K. L. Verosub (1999), Characterizing interactions in fine magnetic particle systems using first order reversal curves, *J. Appl. Phys.*, *85*, 6660–6667, doi:10.1063/1.370176.

Pike, C. R., A. P. Roberts, and K. L. Verosub (2001), First-order reversal curve diagrams and thermal relaxation effects in magnetic particles, *Geophys. J. Int.*, *145*, 721–730, doi:10.1046/j.0956-540x.2001.01419.x.

Reimer, T. O. (1984), Graphite in Precambrian rocks of southern Africa: Implications on the carbon content of metamorphic rocks, *Precambrian Res.*, *26*, 223–234, doi:10.1016/0301-9268(84)90002-0.

Roberts, A. P., and R. Weaver (2005), Multiple mechanisms of remagnetization involving sedimentary greigite (Fe_3S_4), *Earth Planet. Sci. Lett.*, *231*, 263–277, doi:10.1016/j.epsl.2004.11.024.

Roberts, A. P., C. R. Pike, and K. L. Verosub (2000), First-order reversal curve diagrams: A new tool for characterizing the magnetic properties of natural samples, *J. Geophys. Res.*, *105*, 28,461–28,475, doi:10.1029/2000JB900326.

Roberts, A. P., Q. Liu, C. J. Rowan, L. Chang, C. Carvallo, J. Torrent, and C.-S. Horng (2006), Characterization of hematite (α-Fe_2O_3), goethite (α-FeOOH), greigite (Fe_3S_4), and pyrrhotite (Fe_7S_8) using first-order reversal curve diagrams, *J. Geophys. Res.*, *111*, B12S35, doi:10.1029/2006JB004715.

Rochette, P., G. Fillion, J.-L. Mattéi, and M. J. Dekkers (1990), Magnetic transition at 30–34 Kelvin in pyrrhotite: Insight into a widespread occurrence of this mineral in rocks, *Earth Planet. Sci. Lett.*, *98*, 319–328, doi:10.1016/0012-821X(90)90034-U.

Rochette, P., P.-E. Mathé, L. Esteban, H. Rakoto, J.-L. Bouchez, Q. Liu, and J. Torrent (2005), Non-saturation of the defect moment of goethite and fine-grained hematite up to 57 Teslas, *Geophys. Res. Lett.*, *32*, L22309, doi:10.1029/2005GL024196.

Rowan, C. J., and A. P. Roberts (2006), Magnetite dissolution, diachronous greigite formation, and secondary magnetizations from pyrite oxidation: Unravelling complex magnetizations in Neogene marine sediments from New Zealand, *Earth Planet. Sci. Lett.*, *241*, 119–137, doi:10.1016/j.epsl.2005.10.017.

Rowan, C. J., A. P. Roberts, and T. Broadbent (2009), Reductive diagenesis, magnetite dissolution, greigite growth and paleomagnetic smoothing in marine sediments: A new view, *Earth Planet. Sci. Lett.*, *277*, 223–235, doi:10.1016/j.epsl.2008.10.016.

Sakaguchi, A., A. Yanagihara, K. Ujiie, H. Tanaka, and M. Kameyama (2007), Thermal maturity of a fold-thrust belt based on vitrinite reflectance analysis in the Western Foothills complex, western Taiwan, *Tectonophysics*, *443*, 220–232, doi:10.1016/j.tecto.2007.01.017.

Schwertmann, U., and E. Murad (1983), Effect of pH on the formation of goethite and hematite from ferrihydrite, *Clays Clay Miner.*, *31*, 277–284, doi:10.1346/CCMN.1983.0310405.

Song, S.-R., L.-W. Kuo, E.-C. Yeh, C.-Y. Wang, J.-H. Hung, and K.-F. Ma (2007a), Characteristics of the lithology, fault-related rocks and fault zone structures in TCDP Hole-A, *Terr. Atmos. Oceanic Sci.*, *18*, 243–269, doi:10.3319/TAO.2007.18.2.243(TCDP).

Song, Y.-F., et al. (2007b), X-ray beamlines for structural studies at the NSRRC superconducting wavelength shifter, *J. Synchrotron Radiat.*, *14*, 320–325, doi:10.1107/S0909049507021516.

Tanikawa, W., T. Mishima, T. Hirono, W. Lin, T. Shimamoto, W. Soh, and S.-R. Song (2007), High magnetic susceptibility produced in high-velocity frictional tests on core samples from the Chelungpu fault in Taiwan, *Geophys. Res. Lett.*, *34*, L15304, doi:10.1029/2007GL030783.

Tanikawa, W., T. Mishima, T. Hirono, W. Soh, and S.-R. Song (2008), High magnetic susceptibility produced by thermal decomposition of core samples from the Chelungpu fault in Taiwan, *Earth Planet. Sci. Lett.*, *272*, 372–381, doi:10.1016/j.epsl.2008.05.002.

Tribovillard, N., O. Averbuch, A. Bialkowski, and J.-F. Deconinck (2002), Early diagenesis of marine organic-matter and magnetic properties of sedimentary rocks: The role of iron limitation and organic-matter source organisms, *Bull. Soc. Geol. Fr.*, *173*, 295–306, doi:10.2113/173.4.295.

Wang, L., Y. Pan, J. Li, and H. Qin (2008), Magnetic properties related to thermal treatment of pyrite, *Sci. China, Ser. D*, *51*, 1144–1153, doi:10.1007/s11430-008-0083-7.

Wang, P.-L., L.-H. Lin, H.-T. Yu, T.-W. Cheng, S.-R. Song, L.-W. Kuo, E.-C. Yeh, W. Lin, and C.-Y. Wang (2007), Cultivation-based characterization of microbial communities associated with deep sedimentary rocks from Taiwan Chelungpu Drilling Project cores, *Terr. Atmos. Oceanic Sci.*, *18*, 395–412, doi:10.3319/TAO.2007.18.2.395(TCDP).

Wehland, F., A. Stancu, P. Rochette, M. J. Dekkers, and E. Appel (2005), Experimental evaluation of magnetic interaction in pyrrhotite bearing samples, *Phys. Earth Planet. Inter.*, *153*, 181–190, doi:10.1016/j.pepi.2005.05.006.

Wu, H.-Y., K.-F. Ma, M. Zoback, N. Boness, H. Ito, J.-H. Hung, and S. Hickman (2007), Stress orientations of Taiwan Chelungpu-fault Drilling Project (TCDP) Hole-A as observed from geophysical logs, *Geophys. Res. Lett.*, *34*, L01303, doi:10.1029/2006GL028050.

Yeh, E.-C., et al. (2007), Core description and characteristics of fault zones from Hole-A of the Taiwan Chelungpu-fault Drilling Project, *Terr. Atmos. Oceanic Sci.*, *18*, 327–357, doi:10.3319/TAO.2007.18.2.327(TCDP).

Yin, G.-C., Y.-F. Song, M.-T. Tang, F.-R. Chen, K. S. Liang, F. W. Duewer, M. Feser, W. Yun, and H.-P. D. Shieh (2006), 30 nm resolution x-ray imaging at 8 keV using third order diffraction of a zone plate lens objective in a transmission microscope, *Appl. Phys. Lett.*, *89*, 221,122–221,123, doi:10.1063/1.2397483.

Yue, L.-F., J. Suppe, and J.-H. Hung (2005), Structural geology of a classic thrust belt earthquake: The 1999 Chi-Chi earthquake Taiwan (M_w = 7.6), *J. Struct. Geol.*, *27*, 2058–2083, doi:10.1016/j.jsg.2005.05.020.